Materials Science and Engineering C 77 (2017) 583–593

Contents lists available at ScienceDirect

Materials Science and Engineering C

journal homepage: www.elsevier.com/locate/msec

Photothermal conversion efficiency and cytotoxic effect of gold nanorods stabilized with chitosan, alginate and poly(vinyl alcohol)

M. Almada [a], B.H. Leal-Martínez [a], N. Hassan [b], M.J. Kogan [c,d], M.G. Burboa [e], A. Topete [f], M.A. Valdez [a], J. Juárez [a,*]

[a] Departamento de Física, Universidad de Sonora, Hermosillo, Sonora 83000, Mexico
[b] Programa Institucional de Fomento a la Investigación, Desarrollo e Innovación, Universidad Tecnológica Metropolitana (UTEM), Chile
[c] Laboratorio de Nanobiotecnología, Facultad de Ciencias Químicas y Farmacéuticas, Universidad de Chile, Chile
[d] Advanced Center for Chronic Diseases (ACCDiS), Chile
[e] Departamento de Investigaciones Científicas y Tecnológicas, Universidad de Sonora, Rosales y Transversal, 83000 Hermosillo, Sonora, Mexico
[f] Departamento de Fisiología, Centro Universitario de Ciencias de la Salud, Universidad de Guadalajara, Sierra Mojada 950, 44340 Guadalajara, Jalisco, Mexico.

ARTICLE INFO

Article history:
Received 15 November 2016
Received in revised form 2 February 2017
Accepted 23 March 2017
Available online 30 March 2017

Keywords:
Gold nanorods
Photothermal efficiency
Chitosan
Alginate
Cytotoxicity

ABSTRACT

Gold nanorods (GNR) use has been proposed in medical applications because of their intrinsic photothermal properties. However, the presence of CTAB molecules adsorbed onto the surface of GNRs results in a highly cytotoxic GNR system. In this work we replace the CTAB molecules with a thiolated chitosan. Once chitosan coated GNRs (Chi-SH-GNR) were attained, a film of alginate (Alg-Chi-SH-GNR) or polyvinyl alcohol (PVA-Chi-SH-GNR) was deposited onto the surface of Chi-GNR by a layer-by-layer process. The photothermal conversion efficiency for the GNR systems was determined irradiating the GNRs suspended in aqua media with a CW 808 nm diode laser (CNI, China). The cytotoxicity effect and the photothermal cellular damage of GNR systems were evaluated on a breast cancer cell line. Results show that polymer coats did not affect the transduction photothermal efficiency. Values around 50% were obtained for the different coated gold nanorods. The cytotoxicity of coated gold nanorods diminished significantly compared with those GNR stabilized with CTAB. The laser irradiation of cells treated with gold nanorods showed a decrease in their viability compared with the cells treated but no irradiated.

1. Introduction

In the last decades, gold nanoparticles (GNP) have been extensively studied due to their unique optical properties that arise from the surface plasmon resonance phenomena (the collective oscillation of the electron gas due the interaction with the electromagnetic field) [1,2]. When electromagnetic energy is absorbed by GNPs, commonly, a nonradiative mechanism is carried out to dissipate the absorbed energy, inducing a rise in the temperature of the local environment, called photothermic effect. Photothermic properties of GNP systems can be used to promote the death of cancer cells or stimulate the destruction of aberrant functional protein by hyperthermia; this has been called photothermal therapy [3–5].

In particular, gold nanorods (GNRs) are one of most studied nanoparticle systems because of the ease of theirs synthesis in aqueous media [6–9]. Moreover, the experimental protocols used in the synthesis of GNRs allow tuning their surface plasmon resonance into the biological window of the electromagnetic spectrum. Generally, GNRs are synthesized by seed-mediated growth assisted by cetyltrimethylammonium bromide (CTAB), however, it has been demonstrated that the presence of CTAB adsorbed onto the surface of GNRs is related with a high cytotoxicity, limiting the potential use of this nanoparticles in biological applications [10–14]. The excess of CTAB can be eliminated by several steps of centrifugation; although, it is advisable to keep the remaining CTAB absorbed onto the surface of nanorods to avoid the uncontrollable aggregation of gold nanorods [15]. Thus, it is recommendable replace the CTAB by a biocompatible stabilizer to maintain stable the GNR suspension. At this regard, many efforts have been carried out to replace the CTAB from the surface of gold nanorods with different biocompatible and biodegradable polymeric materials in order to enhance the biocompatibility of nanosystems, allowing the use of GNRs in medical fields [16–23]. Polymers, synthetic or natural, such as polyethylene glycol (PEG), polyvinyl alcohol (PVA), chitosan, among others, have been used to stabilize and replace the CTAB from the GNR, the chemical and physical properties of this kind of polymers have been widely used on the preparation of polymeric nanodevices and to overcoat the surface of inorganic nanoparticles [18,21,23–25].

Polysaccharides are ideal candidates to replace the CTAB from gold nanorods surface due to their biocompatibility, low costs and easiness to be modified [26,27]. Furthermore, polysaccharides with poly-

* Corresponding author.
E-mail address: josue.juarez@correo.fisica.uson.mx (J. Juárez).

http://dx.doi.org/10.1016/j.msec.2017.03.218
0928-4931/

electrolytic behavior are suitable to perform a layer-by-layer approach to passivate gold nanorods [22]. In particular, chitosan has been extensively used to replace the CTAB with promising results. For instance, Wang et al. [23] synthesized chitosan-coated gold nanorods. Firstly, mercapto acetic acid (MAA) were covalently attached to amine groups present into the backbone of chitosan via the formation of amide linkage between the amino groups of chitosan and the carboxylate groups of MAA. Thiolated chitosan was incubated for 2 days with CTAB-coated GNRs. The excess of chitosan and CTAB was removed by four cycles of centrifugation-resuspension. Charan et al. [24] replaced the CTAB with 11-mercaptoundecanoic acid (MUA) on the gold nanorod surface, using polyethylene glycol (PEG) as a partial stabilizer. After that, chitosan was attached to the MUA-coated GNRs via carbodiimide reaction. Recently, Yang et al. [25] developed chitosan-GNRs using a layer-by-layer assembled approach, firstly, a layer of the polystyrene sulfonate (PSS) was adsorbed onto the surfaces of CTAB-GNRs obtaining negatively charged particles, in a second step, they used chitosan to overcoat the charged negatively surface of GNRs, inverting the surface charge of nanoparticles to positive.

However, the potential use of chitosan coated GNRs on medicine area is limited by the chitosan behavior in aqueous solutions. Since at physiological pH (7.4) chitosan amino groups (pK ≈ 6.3) are predominantly found deprotonated and, therefore, the surface charge of the nanosystem approaches to zero, affecting the colloidal stability of GNRs [28–30]. Therefore, it arises out of the necessity to coat the chitosan gold nanorod surface with another hydrophilic molecules or polymers to stabilize the GNR system [30]. In this work we used two biocompatible and hydrophilic polymers to stabilize a chitosan coated GNRs (Chi-GNR) to enhance their potential use in the medicine area as photothermic agent. Sodium alginate (anionic polymer) or PVA (hydrophilic non-ionic polymer) were used to overcoat the chitosan layer of GNRs, allowing to get a stable Chi-GNRs suspension at physiological pH. It is worth mentioning that alginate and PVA supply of biocompatible properties to GNRs systems, as was demonstrated by the in vitro cellular assays. The polymer coating process was performed in two sequential steps, first, thiolated chitosan was adsorbed onto the surface of GNR and, in a second step, chitosan-coated GNRs were overcoat with alginate or PVA. Interestingly, the chitosan, alginate or PVA coated, did not affect the photothermal conversion efficiency (η) of GNR systems (Chi-GNR, Alg-Chi-GNR and PVA-Chi-GNR). The η values resulted similar and comparable to the CTAB-coated GNRs. Finally, we evaluated their cytotoxicity on a breast cancer cell line with and without laser irradiation (CW 808 nm diode laser (CNI, China)). These results support the potential use of these GNR systems as photothermic agent due to the increment of the cellular damage observed when cell samples were irradiated in presence of the polymer-coated GNRs.

2. Materials and methods

2.1. Materials

Chitosan oligosaccharide lactate (Mn 5000), Alginic acid sodium salt from brown algae (low viscosity), Poly (vinyl alcohol) (Mw ~31,000, 86.7–88.7 mol% hydrolysis), *N*-(3-Dimethylaminopropyl)-*N*′-ethylcarbodiimide (EDC), *N*-Hydroxysuccinimide (NHS), *N*,*N*-Dimethylformamide (DMF), 3-Mercaptopropionic acid, Hexadecyltrimethylammonium bromide (CTAB), Hydrogen tetrachloroaurate(III) ($HAuCl_4$), Silver Nitrate ($AgNO_3$), Ascorbic acid and Sodium tetrahydridoborate ($NaBH_4$) were obtained from Sigma Aldrich and they were used as received.

2.2. Gold nanorods synthesis

Gold nanorods were synthesized by the well-known seed-mediated method [7] at low pH [31,32]. All glassware was cleaned by aqua regia before using it to remove any contamination. The gold seeds were prepared by adding 0.5 ml of $NaBH_4$ solution (10 mM), previously dissolved in ice-cold water, to 5 ml of an aqueous solution composed of CTAB (0.1 M) and $HAuCl_4$ (0.48 mM). This solution was stirred vigorously for 2 min and then was kept undisturbed at 33 °C for 30 min. The growth solution was prepared separately by mixing CTAB, HCl, $HAuCl_4$, $AgNO_3$ and Ascorbic acid with concentrations in the final mixture (100 ml) of 0.1 M, 0.08 M, 0.5 mM, 0.085 mM and 1 mM, respectively. The colorless growth solution was kept at 33 °C and after 30 min 100 μl of seed solution was added [32].

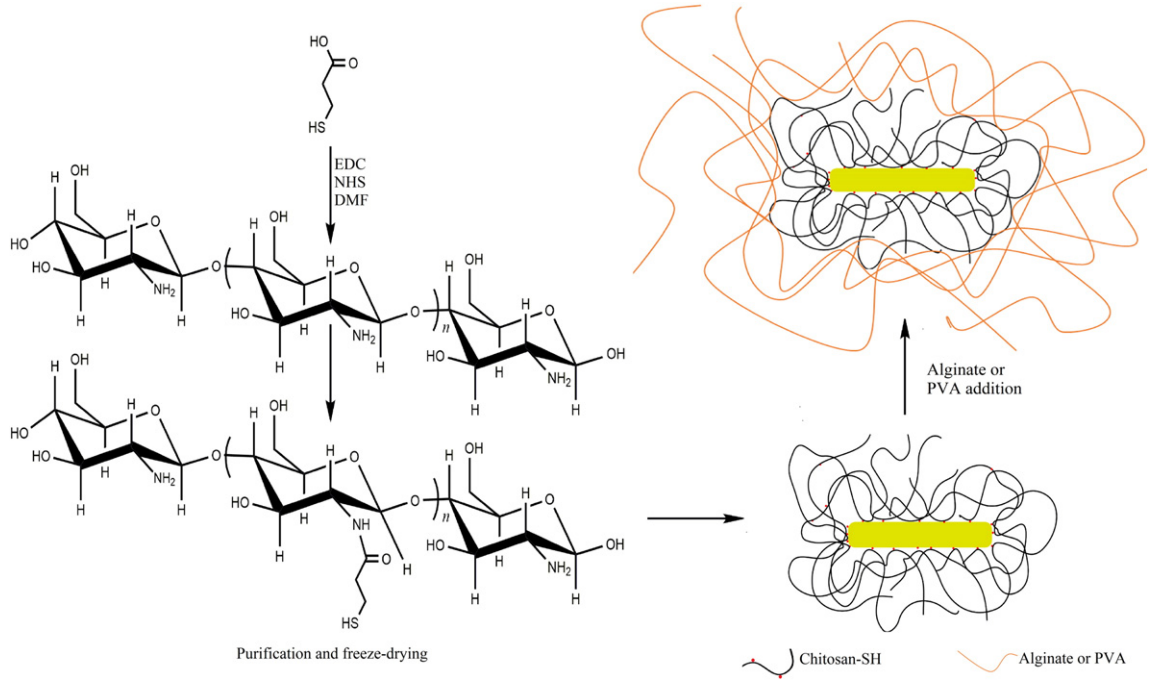

Scheme 1. Synthesis process of polymers-coated gold nanorods.

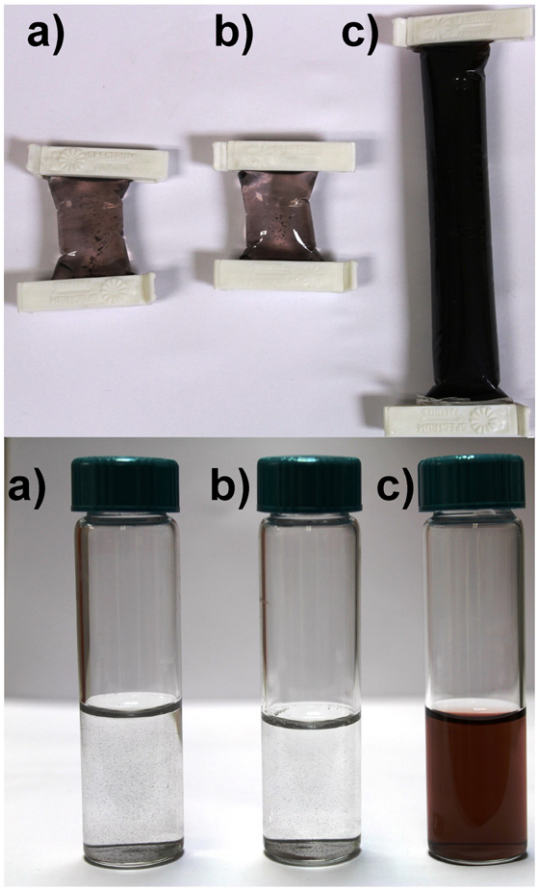

Fig. 1. GNRs after dialysis: a) CTAB-GNRs, b) PEG-SH-GNRs and c) Chi-SH-GNRs.

2.3. Thiol-Chitosan (Chi-SH) synthesis

Thiol-Chitosan (Chi-SH) was obtained according to the protocol described by Zhu et al. [33]. Covalent attachment of 3-Mercaptopropionic acid (MPA) to chitosan backbone was achieved by the formation of amide bonds between amino groups of chitosan and the carboxylic groups of the MPA. Firstly, the carboxylate groups of 3-Mercaptopropionic acid were activated by mixing 21 mg of MPA, 13 mg of EDC and 15 mg of NHS in 2 ml of Dimethylformamide (DMF), and then this solution was added to 40 ml of 2.5% chitosan solution in HCl 0.1 M (pH 5.5). This solution was stirred for 5 h and then washed 3-times with ethanol; finally, the product was lyophilized and stored at room temperature. FTIR spectrum of thiolated chitosan obtained is shown in Fig. S1.

2.4. Chi-SH-coated gold nanorods synthesis

Gold nanorods were washed by centrifugation twice to eliminate the CTBA excess and were suspended in 10 ml (10% of the initial volume) of water. Then, 10 mL of Chi-SH solution (1 mg/ml in HCl 0.1 M) was added to gold nanorods suspensions and the final mixture was stirred by 3 h. Finally, the chitosan-coated gold nanorod suspension was dialyzed by two days against HCl 0.01 M.

2.5. PEG-SH-coated gold nanorods synthesis

We used a traditional method for PEG-SH coating of GNRs: 10 ml of pre-synthesized gold nanorods were centrifuged twice to eliminate the CTAB excess. Then GNRs were re-dispersed in a 10 mM CTAB solution (10 ml) and sodium carbonate (1 ml, 2 mM) and PEG–SH (100–500 μL, 2 μM, 5000 Da) was sequentially added to the GNR solution. Finally, the solution was magnetically stirred at room temperature for 24 h [19, 20].

2.6. PVA and alginate coated chitosan-gold nanorods

A layer by layer approach was used to overcoat the Chi-SH-coated gold nanorods (Chi-GNR). Briefly, 0.5 ml of GNRs suspension obtained after dialysis was added by dropwise under magnetic stirring into 0.5 ml of PVA or alginate solutions at 1% and 0.5 mg/ml, respectively. After 10 min, the suspension was centrifuged at 6000 rpm for 30 min and the pellet was re-suspended in water (the entire process is depicted in Scheme 1).

2.7. Infrared spectroscopy

Polymer coated GNRs and CTAB-GNRs were centrifuged and suspended in water twice to eliminate the excess of polymer or surfactant, samples were lyophilized and the spectrums were obtained in ATR mode using a Perkin Elmer Spectrum Two instrument.

2.8. Zeta potential

Zeta potential of NPs was measured by using a Nano ZS (Nanoseries, Malvern Instruments, UK). Gold nanorods were suspended in water (pH ~ 5) or phosphate buffer 10 mM (pH = 7.4) and fed into a folded capillary, clear, disposable zeta cell. Zeta potential is reported as the mean ± standard deviation (SD) of three independent measurements.

2.9. Transmission electron microscopy images

Gold nanorods suspension (10 μl) was deposited onto a copper grid and was dried overnight. TEM images were acquired using Phillips CM-12 Instrument.

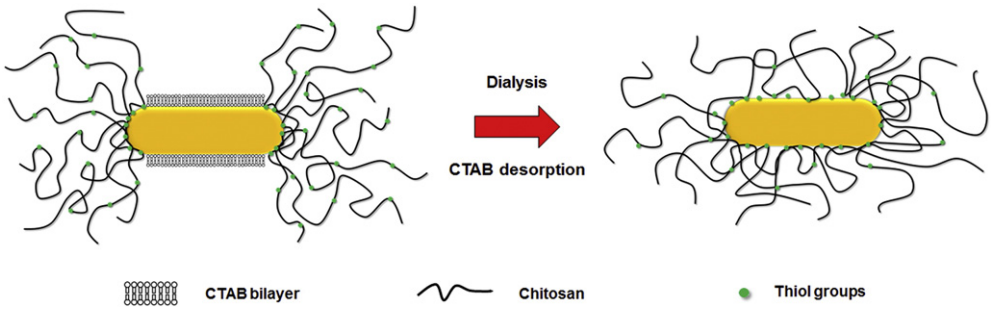

Fig. 2. Schematic representation of GNRs chitosan coating process.

2.10. Atomic force microscopy images

A JEOL instrument (JSPM 4210, Japan) was used for imaging. 10 μl of diluted gold nanorods suspensions were deposited on freshly cleaved mica and left drying, the images were obtained in the noncontact mode using silicon nitride cantilevers (NSC15) from MicroMash (USA).

2.11. Photothermic experiments

Photothermal properties of GNRs coated with CTAB, chitosan-SH, alginate and PVA were assessed adding 3 ml of GNRs solution into a spectroscopic quartz cuvette. GNRs solutions were prepared at different optical densities (2, 1, 0.50 and 0.25) and the samples were irradiated with a CW 808 nm diode laser (CNI, China). The temperature of the sample was followed with a *k* type thermocouple connected to a digital thermometer (AMPROBE TMD-51). The sensor temperature probe was inserted into the bulk solution and the cuvette was sealed to avoid evaporation. The sample was illuminated using different powers 2 W, 1.5 W and 1 W over a period of 40 min, recording the temperature every 30 s.

2.12. Photothermal conversion efficiency

The photothermal conversion efficiency (η) was determined using a model described previously [34]. The temperature increase of the solution can be determined by the balance between the heat rate input from the laser via the nanorods, (Q_I), to the quartz cuvette-water system, (Q_0), and the heat dissipation rate to the external environment by convection, (Q_{ext}), that can be expressed by:

$$\sum_i m_i C_i \frac{dT}{dt} = Q_I + Q_0 - Q_{ext} \tag{1}$$

where m_i and C_i are the mass and specific heat capacity of component *i*, respectively. *T* is the temperature, and *t* is time. The term Q_I corresponds to the heat dissipated by electron-phonon relaxation process of surface plasmons of GNRs induced by laser irradiation at a resonant wavelength λ to the solution and it can be expressed by:

$$Q_I = I\left(1-10^{-A\lambda}\right)\eta \tag{2}$$

where *I* is the incident laser power, η represents the efficiency of transducing incident resonant light to thermal energy (it means the portion of light that is absorbed by particles), and $A\lambda$ is the absorbance of nanorods at a certain wavelength (in this case the absorbance at 808 nm). The term Q_0 corresponds to the heat produced by the laser over the cuvette and water and it can be determined illuminating the system without nanorods. Heat dissipated to the external environment (Q_{ext}) is given by:

$$Q_{ext} = hA(T - T_{amb}) \tag{3}$$

where *h* is the heat transfer efficiency, *A* is the surface area of the interface between the nanorods solution and external environment. Then we can re-write the Eq. (1) as:

$$\sum_i m_i C_i \frac{dT}{dt} = I\left(1-10^{-A\lambda}\right)\eta + Q_0 - hA(T - T_{amb}) \tag{4}$$

For simplicity Roper et al. [34] defined a characteristic rate constant or sample system time constant (τ_s) as:

$$\tau_s \equiv \frac{\sum_i m_i C_i}{hA} \tag{5}$$

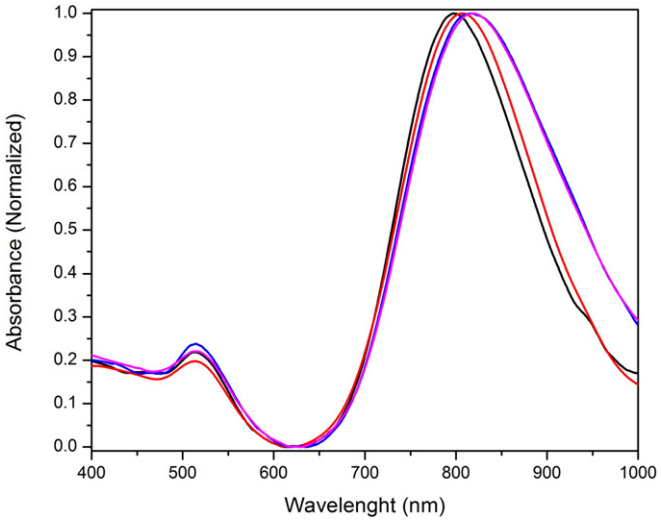

Fig. 3. GNRs UV–Vis spectrums. CTAB-GNRs (black line), Chi-SH-GNRs (red line), Alg-Chi-SH-GNRs (blue line), PVA-Chi-SH-GNR (Magenta line).

Taking into account the Eqs. (4) and (5) and considering $\Delta T = (T - T_{amb})$, we can resolve the differential equation to obtain:

$$\Delta T(t) \equiv \tau_s \left[\frac{I\left(1-10^{-A\lambda}\right)\eta + Q_0}{\sum_i m_i C_i}\right]\left(1-e^{-t/\tau_s}\right) \tag{6}$$

This equation is used to obtain τ_s and η, simply, by fitting the heating experimental data, in order to calculate Q_0 value the fitting must be done on the curve of heating without nanorods, in this case $Q_I = 0$ and the equation is simplified to:

$$\Delta T(t) \equiv \tau_s \left[\frac{Q_0}{\sum_i m_i C_i}\right]\left(1-e^{-t/\tau_s}\right) \tag{7}$$

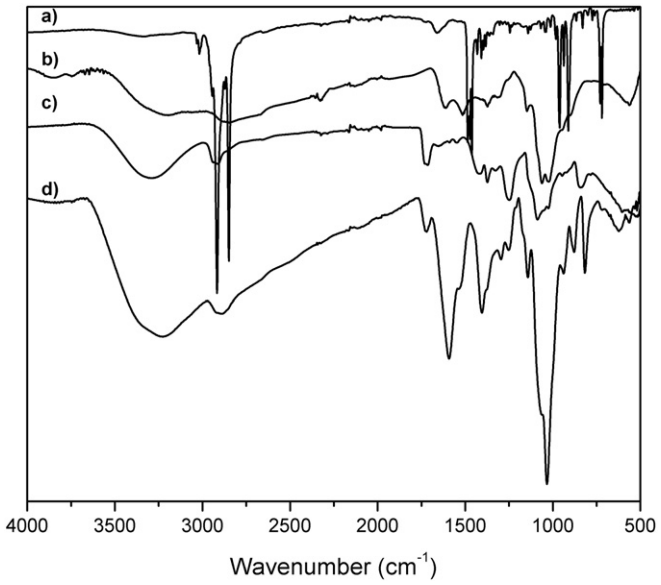

Fig. 4. Infrared spectrums of GNRs. a) CTAB-GNRs, b) Chi-SH-GNRs, c) PVA-Chi-SH-GNR, d) Alg-Chi-SH-GNRs.

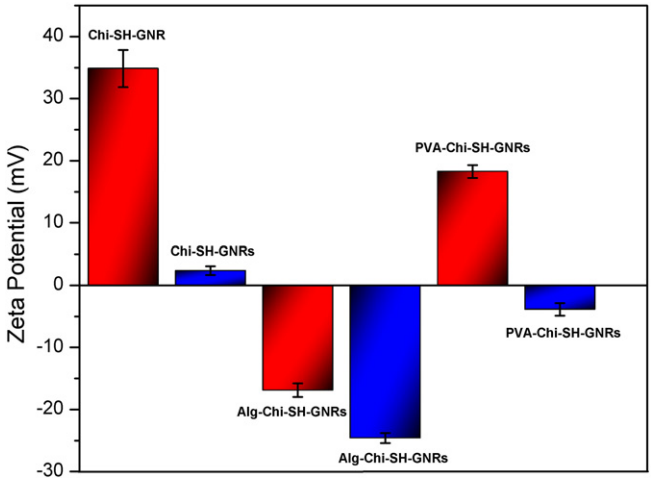

Fig. 5. Zeta potential of GNRs in water at pH ≈ 5 (red) and in phosphate buffer at pH of 7.4 (blue).

2.13. Cytotoxic assays

Breast cancer cells line MDA-MB-231 was used as a cellular model in order to assess the cytotoxic effect of gold nanorods. Cell line was cultured in Dulbecco's modified Eagle medium (DMEM) with fetal bovine serum (15%), 100 U/ml penicillin and 100 g/ml streptomycin; Cultures were incubated at 37C, 5% CO_2 and 90% humidity.

The cytotoxic activity of gold nanorods, PVA and alginate with and without irradiation was evaluated by the MTT reduction method. The cells were seeded in 96-well plates at a density of 5×10^3 cells/well. After 24 h incubation, cells were treated with gold nanorods at concentrations of 4.8×10^{10}, 3.6×10^{10}, 2.4×10^{10} and 1.2×10^{10} particles/ml (these concentrations of GNR were calculated using an extinction coefficient of $5 \times 10^{-9}\ M^{-1}\ cm^1$ for a GNR with an aspect ratio of around 3.8 [35–38]. The optical densities of GNR suspensions were adjusted to 0.4, 0.3, 0.2 y 0.1, respectively), or polymers at concentrations of 1.0, 0.50, 0.25 and 0.125 mg/ml. In the case of irradiation assays the same gold nanorods concentrations were used and the cell cultures were illuminated by 5 min with 808 nm laser. The cytotoxicity was measured after 48 h adding 10 μl of MTT at each well and incubating for 4 h. 100 μl of acidic isopropanol was added to solubilize the formazan salts formed and the optical density was measured at 570 nm. Relative cell

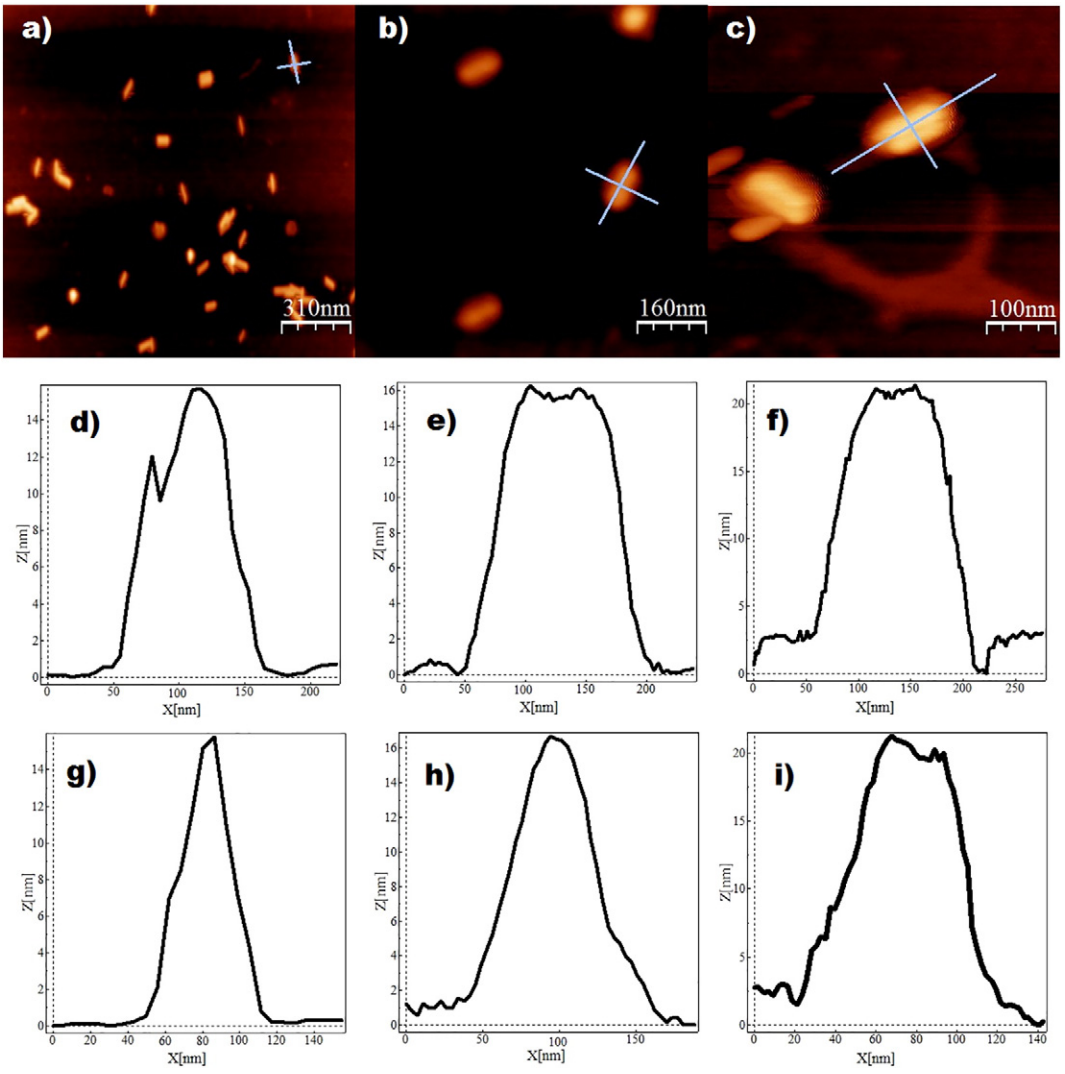

Fig. 6. AFM images and representative longitudinal and transverse profiles of GNRs; a) Chi-SH-GNRs, b) Alg-Chi-SH-GNRs, c) PVA-Chi-SH-GNRs, d), e) and f) representative longitudinal profile, g), h) and i) representative transversal profile (each profile corresponds to the top AFM image).

viability was determined by the amount of MTT converted into formazan and calculated as a percentage compared to the control group.

3. Results and discussion

3.1. Chitosan-SH-coated gold nanorods synthesis

In this work we used a very easy and reproducible method to eliminate the CTAB using thiolated chitosan as stabilizer of GNRs. We employed a method based in dialysis for the CTAB elimination and, at the same time, as preliminary proof to determine if the polymer coating had been attained adequately. Fig. 1 shows the CTAB-GNR and thiol-polyethylene glycol-GNR (PEG-SH-GNR) solutions after 3 h of dialysis, and the Chitosan-GNR (Chi-GNR) solution after 48 h of dialysis. We can observe the usefulness of thiolated chitosan to remove the CTAB from the GNR surface stabilizing the chitosan-GNR solution even after 48 h of dialysis. In contrast, the CTAB-GNR and PEG-SH-GNR suspension become unstable and form aggregates over a period of 3 h. The instability observed in the CTAB-GNRs is a consequence of the CTAB diffusion from the GNRs surface to outside of the dialysis bag. In the case of PEG-SH coated process, we expected to obtain a stable GNR suspension due to the adsorption of thiolated PEG onto the surface of GNR, however, GNR form aggregates during the dialysis process, as in the case of CTBA-GNRs. We suggest that CTAB molecules adsorbed on the lateral facet of GNRs allow the covalent attachment of small amount of PEG-SH molecules. This behavior agrees with previous reports where it has been demonstrated that thiolated molecules preferentially interact with the end-tip surface of GNRs, while CTAB molecules remain attached onto the lateral facets of GNRs [39–43]. Thus, when the concentration of CTAB decreases during the dialysis process, the PEG-SH attached onto the GNRs surface is not enough to stabilize the colloidal system.

When Chi-SH is used to stabilize the GNRs in aqueous solution no agglomeration was observed even after long periods of dialysis. We suggested that thiol groups attached along the polymer chain play a pivotal role in the successful replacement of CTAB linked onto the GNR surface. Similar to the PEG-SH coating process previously reported, during the coated process of GNRs, Chi-SH molecules bind onto the end-tip surface of GNRs through the thiol groups localized around the media section of the chitosan chain, leaving free two lateral arms of the Chi-SH (Fig. 2). We must take into account that at this step there still exist CTAB molecules adsorbed onto the lateral surface facets of GNRs that avoid the attachment of remaining arms of Chi-SH. During the dialysis process, CTAB molecules left the GNR surface leaving the lateral surface sides of GNRs available for the adsorption of Chi-SH arms and additional Chi-SH molecules are binding. We suggest that desorption process of CTAB occurs progressively and slowly, allowing the attachment of thiolated chitosan arms, as well as additional thiolated chitosan molecules, until CTAB molecules are completely replaced by Chi-SH. Protonated chitosan amino groups promote the electrostatic stabilization of GNRs suspension (pH $\approx$ 4) for a large period time.

Fig. 3 shows the UV–Vis spectra of CTAB-GNR and Chi-SH-GNR. We can observe a slight red shift of 9 nm of the longitudinal surface plasmon resonance (from 798 nm to 807 nm) when thiolated chitosan was

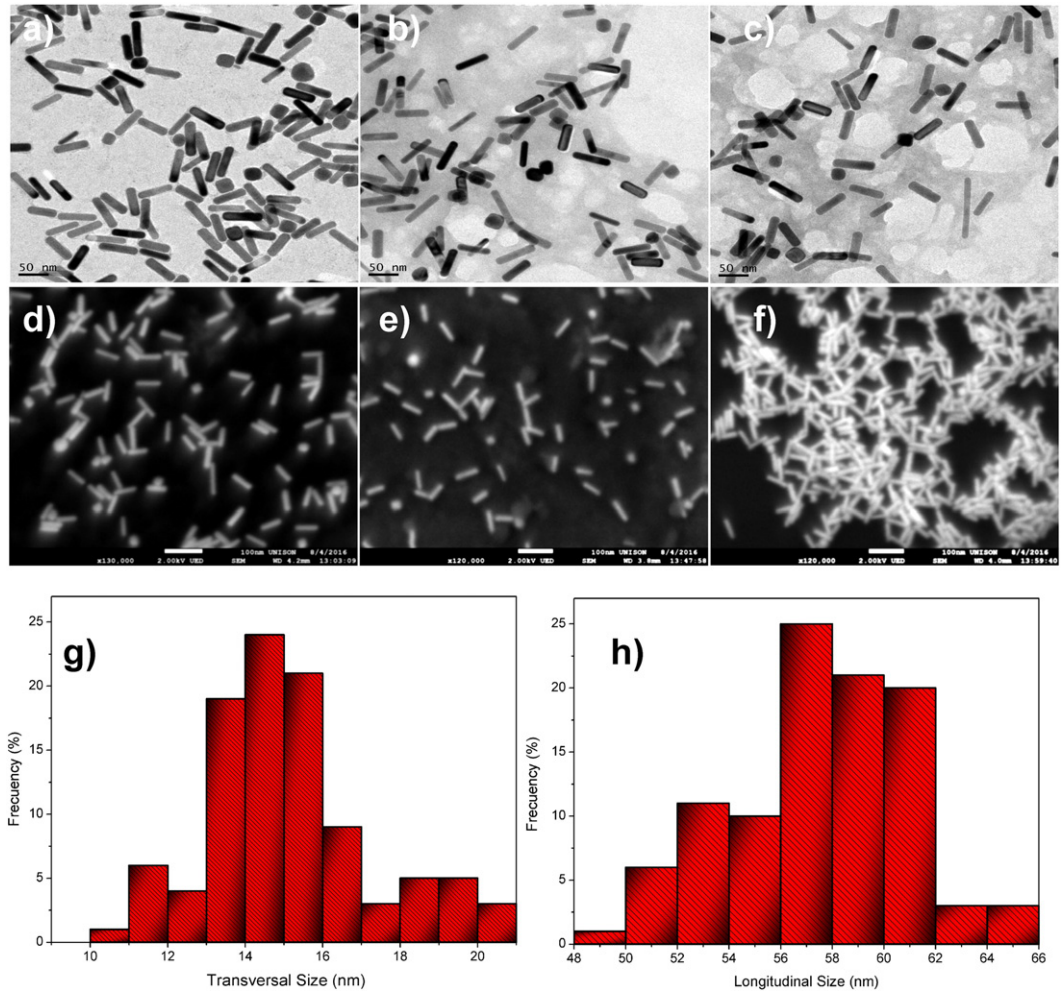

Fig. 7. TEM and SEM images of GNRs; a) and d) Chi-SH-GNRs, b) and e) Alg-Chi-SH-GNRs, c) and f) PVA-Chi-SH-GNRs and transversal and longitudinal size of GNRs, g) frequency histogram of transversal size, h) frequency histogram of longitudinal size. (Scale bar in SEM images 100 nm.)

attached onto the GNR surface. This behavior has been previously reported (using different polymers) and it has been suggested that this phenomenon can be attributed to the local refractive index change due to the presence of the organic polyelectrolyte [44–47].

3.2. PVA and alginate coated gold nanorods

Layer by layer approach has been used previously to passivate, tune, and/or invert the surface charge of GNRs synthetized in presence of CTAB. For instance, polyelectrolytes as polystyrene sulfonate (PSS) and poly(diallyldimethylammonium chloride) (PDADMAC) have been deposited in serial sequence steps. Firstly, a layer of the anionic polymer (PSS) was deposited over the CTAB layer, changing the zeta potential to negative. After that, the PDADMAC, cationic polymer, was adsorbed onto the negative surface charge of the PSS coated GNR. This process can be repeated to obtain a polymeric multilayer nanosystem [46,47]. On the base of these previous reports, we replaced the CTAB with thiolated chitosan and, after this step, an alginate (anionic polymer) or PVA (nonionic polymer) layer was deposited onto the Chi-SH-GNR surface. Fig. 3 shows the UV–Vis spectra of Chi-SH-GNRs before and after modifying their surface with alginate or PVA using a layer-by-layer process. We observed an additional red-shift, around 9 nm, for either PVA or Alg was adsorbed onto the surface of Chi-SH-GNR. Similar results were observed in previous research works, in which polymeric multilayers were deposited onto the surface of gold nanoparticles [46,47]; UV–Vis spectra showed a red-shift of the surface plasmon band for each polymeric layer deposited in a sequential process. The red-shift observed after polymeric layers deposition onto the nanoparticle surface has been attributed to the local environment changes around the gold nanoparticle surface, modifying the plasmon resonance response upon incident electromagnetic radiation. UV–Vis spectra of coated GNRs in PBS, DMEM and DMEM media supplemented with 10% of fetal bovine serum are shown in Supplementary information (S2–S4), absorption spectra demonstrated that Chi-SH-GNR suspensions are unstable in the three supplemented media. Since after few minutes, we observed the aggregate formation of GNRs at the bottom of glass vial. This behavior is due to deprotonation of amino groups of chitosan at physiological pH (7.4), diminishing the electrostatic repulsion between Chi-SH-GNR. In contrast Alg-Chi-SH-GNRs and PVA-Chi-SH-GNRs spectra show that these GNR systems are stable in the three media, due to the high electrostatic repulsion of deprotonated carboxylic groups of alginate and to the steric stabilization of PVA, respectively. These results show that Alg-Chi-SH-GNRs and PVA-Chi-SH-GNRs have a potential use in the medicine areas.

The FTIR spectra recorded from GNRs are shown in Fig. 4. Fig. 4a shows the CTAB-GNRs spectrum, the intense peaks at 1480 cm^{-1} and 2800–2900 cm^{-1} corresponded to bending and stretching of C—H bonds and the peaks at 910, 964 and the doublet at 725 cm^{-1} can be assigned to the wagging of C—N bonds [48,49]. Fig. 4b corresponds to the FTIR spectrum for Chi-SH-GNRs; we can observe that intense peaks of the CTAB are replaced by the characteristic band of chitosan. The broad band located around 3200 cm^{-1} has been associated with the stretching of $-NH_2$ and $-OH$ groups, peaks located around 1517 and 1620 cm^{-1} are attributed to N—H bending, and the C—O and C—O—C stretching, of the secondary alcohols and glycoside bonds of the polysaccharide structure, appeared between 950 and 1100 cm^{-1} [50–52], respectively. The PVA-Chi-SH-GNR spectrum is shown in Fig. 4c, a broadening in the band at 3300 cm^{-1} is observed due to the presence of $-OH$ on the structure of PVA, the peak at 1730 can be due the stretching to C═O from acetate group remaining in PVA (we used PVA with 86.7–88.7 mol% hydrolysis) [53]. Fig. 4d corresponds to the FTIR spectrum recorded for Alg-Chi-SH-GNRs. Two important peaks at 1600 and 1400 cm^{-1} can be observed which can be assigned to the antisymmetric and symmetric carboxylate stretch of the alginate, respectively [54]. On the base of these results we can confirm that CTAB molecules adsorbed on the GNR surface were successfully replaced by

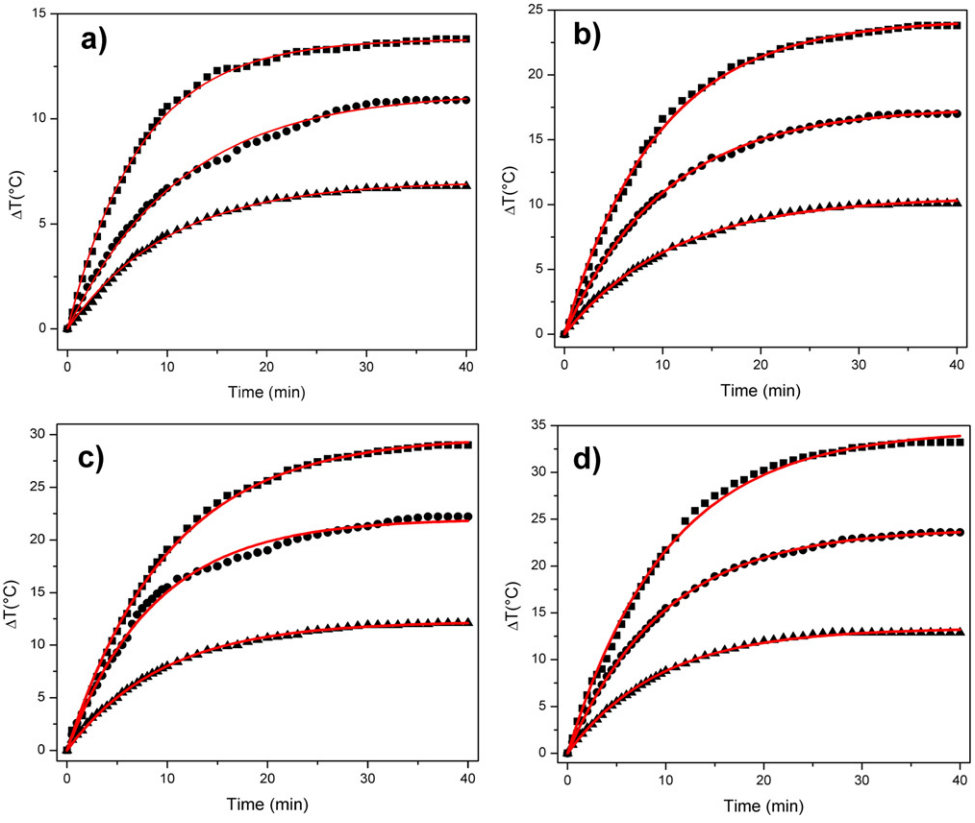

Fig. 8. Heating profile for Alg-Chi-SH-GNRs at different absorbance values a) 0.25, b) 0.5, c) 1.0, d) 2.0; and laser powers of 1 W (▲), 1.5 W (●) and 2.0 W (■). The solid red line correspond the data fit with Eq. (6).

thiolate chitosan molecules and the deposition layer of alginate or PVA was adsorbed on the surface of Chi-SH-GNRs.

On the other hand, the surfaces charge of polymer coated GNRs were followed by zeta potential (ζ) measurement. It is important to note that ζ measurements were done in aqueous media at pH ≈ 5.0 to ensure that amino groups exposed on the surface of Chi-SH-GNRs remained protonated. Then, changes on surface charge values were used as a parameter to confirm if the Chi-SH-GNRs had been covered by PVA or alginate. Results are summarized in Fig. 5. We can observe an inversion of the positively charged surface of Chi-SH-GNRs (ζ +35 mV), after the deposition of alginate layer (ζ −17 mV). For the case of the PVA coating, the zeta potential diminished to +18 mV. This behavior can be explained on the basis of ionization characteristics of the polymer used to overcoat the Chi-SH-GNR at pH 5.0; the pKa of carboxylic groups linked along the chain of alginate is around pH ≈ 3.5, therefore, these carboxylic groups are ionized and the alginate molecules are negatively charged [55]. Carboxylic groups of the anionic alginate allowed the electrostatic association with the amino groups exposed on the chitosan layer, leading to a reversal surface charge of the nanoparticle from positive values, for Chi-SH-GNRs, to negative values, for Alg-Chi-SH-GNRs. PVA, characterized as polar and non-ionic polymer, has hydroxyl functional groups that promoted the adsorption over the chitosan layer adsorbed onto the surface of GNPs through of stablishing hydrogen bonds between PVA and chitosan. Thus, chitosan electric charges are screened by PVA molecules and a reduction of zeta potential is observed, without reversal of surface charge.

At pH ≈ 7.4 (10 mM phosphate buffer) Chi-GNRs, Alg-Chi-SH-GNRs and PVA-Chi-SH-GNRs showed zeta potential values around +2 mV, −24 mV and −3 mV, respectively; Chi-SH-GNRs presents this behavior due to the deprotonation of amino groups (pK ≈ 6.3) that diminished the surface charge of particles [28–30], and the precipitation of Chi-SH-GNRs under these conditions is observed after a few minutes. For the case of Alg-Chi-SH-GNRs, the more negative zeta potential observed is probably due to deprotonation of carboxylic groups because of the pH increment [56]; PVA-Chi-SH-GNRs shows a zeta potential slightly more negative (−3 mV) when these particles are dispersed in the buffer, we suggested that the diminishing of the surface charge is due to the adsorption of phosphate ions onto the amino groups exposed outside to PVA-Chi-SH layer forming the Stern layer around the PVA-Chi-SH-GNRs. However, the GNRs suspension remains still stable due to steric interaction provided by PVA.

We further confirmed the layers deposition over the Chi-SH-GNRs using AFM images. In Fig. 6 images of Chi-GNRs, Alg-Chi-SH-GNRs and PVA-Chi-SH-GNRs are shown together with a representative profile. The longitudinal and transversal size can be visualized; in accord to AFM images, Chi-SH-GNRs have a longitudinal and transversal size around 100 nm and 50 nm, respectively. In the case of Alg-Chi-SH-GNRs and PVA-Chi-SH-GNRs we observed a size increment around 50 nm in comparison with Chi-SH-GNR over both longitudinal and transversal size. However, polymer coated GNRs observed by TEM and SEM images showed a longitudinal and transversal size around 57 nm and 15 nm (aspect ratio 3.8, Fig. 7), respectively. We can explain this great difference in size observed by AFM and electronic microscopy (TEM and SEM) on the base of the basic function of these equipments. Additionally, we must consider that polymer coated GNRs tend to form aggregates as result of the dehydration of samples. Thus, AFM images show the surface relief sensed by a probe that scans the surface of polymer coated GNR aggregates. While TEM and SEM images showed the metallic core of polymer coated GNR aggregates, because the polymeric layers are transparent or semitransparent to the electron beam used in both electronic microscopies.

3.3. Photothermal conversion efficiency (η)

Photothermal conversion properties for the four GNR systems were determined under experimental conditions previously described in materials and methods section. Previously, Roper et al. [34] demonstrated that it is possible to predict the maximum equilibrium temperature changes, which is proportional to the nanoparticle concentration, using a heat-transfer model (Eq. (6)). We determined the photothermal transduction efficiency (η) by fitting experimental data with Eq. (6). It is important to note that the characteristic rate constant, (τ_s), depends on the experimental array, while η can be considered as an intrinsic property of gold nanoparticles and, therefore, photothermal transduction efficiency only depends on the shape and size of GNRs [37,57–59]. As the absorbance of gold nanoparticles corresponds to the absorption light and scattering light [37], we considered that the η values could be affected by the attachment of polymeric layers onto the surface of the GNRs, diminishing the efficacy of the photothermal transduction by the enhancing of the scattered light. Under this consideration, we determined the value for τ_s and η for CTAB-GNR, Chi-SH-GNR, Alg-Chi-SH-GNR and PVA-Chi-SH-GNR by fitting the experimental heating data with Eq. (6). Fig. 8 shows the heating profiles observed for Alg-Chi-SH-GNR solution, varying the amount of GNR into solution (absorbance) and laser power irradiation. A Similar heating profile was observed for all GNR system (Supporting information S5–S7). Heating data recorded adjusted

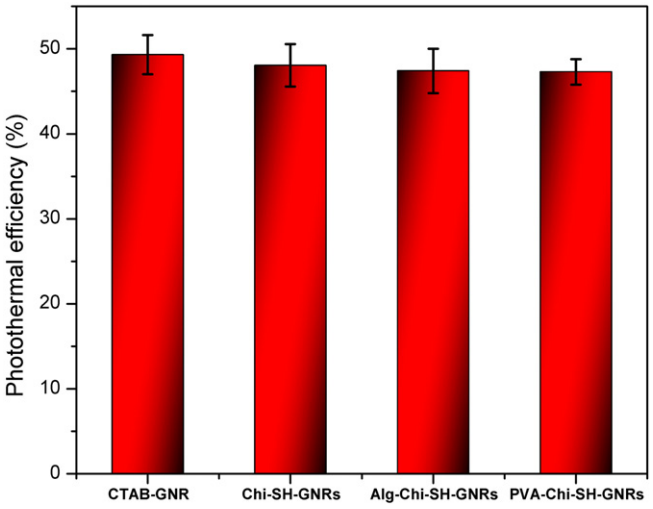

Fig. 9. Photothermal efficiency (η) of GNRs covered with different polymers. (The average and standard deviation was obtained considering all experimental data fitting; we assume that η is independent from GNRs absorbance and laser power usEd.)

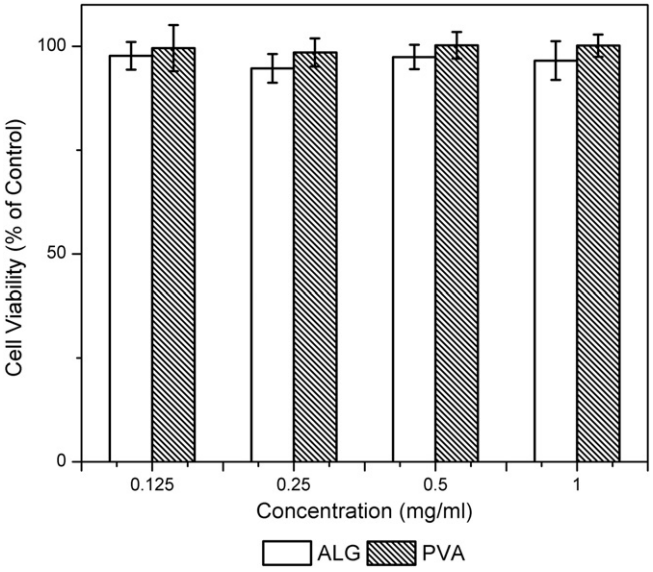

Fig. 10. Cell viability of MDA-MB-231 line treated with polymers alginate and PVA.

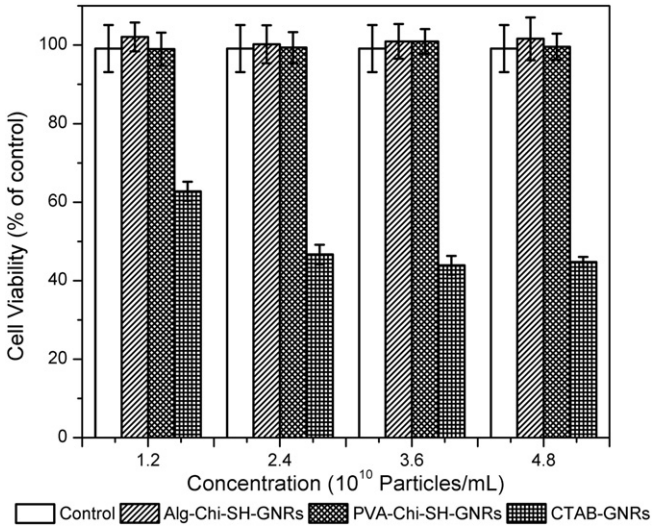

Fig. 11. Cell viability of MDA-MB-231 line treated with GNRs.

adequately to the theoretical non-linear curve fit (solid line) Eq. (6). We observed a high increment of the temperature at the first minutes of irradiation until a saturation temperature (plateau) is attained and, after that, the temperature increment is negligible (Fig. 8), in accordance with previous reports [34,57,58,60]. The characteristic rate constant (τ_s) and photothermal transduction efficiency were attained from heating profiles and, they showed practically constant values, around 9.4–10.2 min for the τ_s and 0.47–0.51 for η. The average η values for each type of GNRs used in this work is shown in Fig. 9, these results are similar to those previously reported by Pattani et al. [8] and Cole et al. [60]. They reported a η of 50% and 55% for nanorods with size of 7×26 nm (LSPR 770 nm), using an 808 nm laser and for gold nanorods with size of 13×44 nm (LSPR 780 nm) using an 815 nm laser, respectively. η can be understood as the absorption/extinction ratio and is often used to describe the efficiency of the nanoparticles to convert light into heat; in this sense, these results indicate that the 50% of the light extinction by these GNRs is transformed into heat. It is worth to mention that η values determined for the three GNR systems are negligible, suggesting that polymer coat does not affect the GNRs capacity to transform the electromagnetic radiation into heat, contrary to the supposition postulated before to initiate the photothermal experiment. We propose that the polymeric layers deposited onto the GNR surface is transparent to the wavelength used in the irradiation experiment and, moreover, the polymeric layer is thin enough to enhance the scattered light contribution on the extinction of GNR and, therefore, the η observed for the different GNR systems resulted similar. We considered this fact as positive result because polymeric coated GNRs could be used in the fabrication of a photothermal nanosystem with potential application in medical area. With this purpose, we evaluated the photothermic properties of Chi-SH-GNR, Alg-Chi-SH-GNR and Chi-SH-GNR, and their capacity to produce cellular damage in vitro. Results are described in the following section.

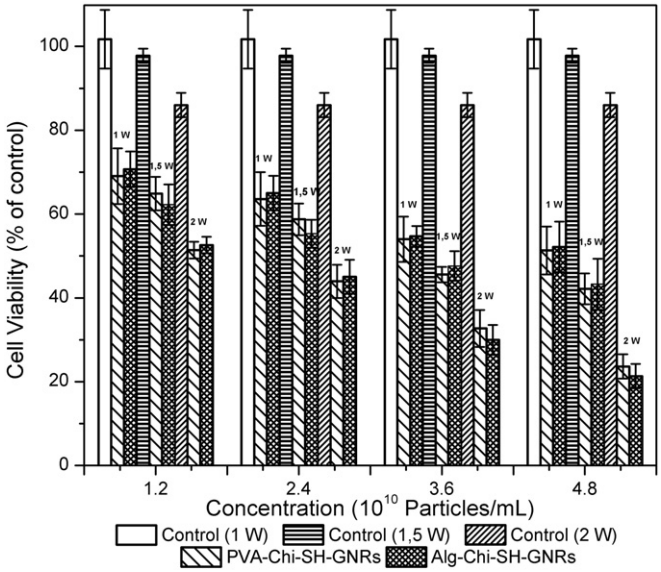

Fig. 12. Cell viability of MDA-MB-231 cell line treated with GNRs and irradiation.

3.4. Cytotoxic assays

GNRs have been proposed to be useful in diagnostic and treatment of cancer [61], however, it has been demonstrated that these particles exhibit high cytotoxicity which is independent of the GNRs itself but is due to the CTAB molecules on their surface, this limits their use in medical applications. This cytotoxicity can be significantly diminished trough the passivating or elimination of these molecules from de GNRs surface using diverse polymers [14]. This has been previously attained using polyacrylic acid (PAA), polystyrene sulfonate (PSS), polyallylamine (PAH) and chitosan; the cytotoxicity is diminished even if the surface is negatively or positively charged [11,14,24].

In this work we use chitosan, alginate and PVA to coat the GNRs; the three polymers are considered biocompatible [62–64]. In Fig. 10 the cytotoxicity of PVA and alginate on MDA-MB-231 cell line is shown, it is clearly observed that the two polymers did not affect the cell viability even at concentrations as high as 1 mg/ml. GNRs cytotoxicity is shown in Fig. 11, polymers coated GNRs cytotoxicity is significantly lower than CTAB-GNRs, these results agree with literature, i.e., GNRs cytotoxicity is due mainly the CTAB molecules presents in GNRs suspension and not to an intrinsic effect of GNRs.

Fig. 12 shows the cytotoxic effect of GNRs after irradiation at different laser powers; it can be observed at first instance that the laser power of 2 W diminished significantly cell viability (viability around 82%) while the irradiation with 1 W and 1.5 W did not affect the cell survival. Negligible differences in cytotoxicity were observed between Alg-Chi-SH-GNRs and PVA-Chi-SH-GNRs for the three laser powers used, which agree with the results from Fig. 9 where no differences on the photothermal efficiency transduction were noticed between them. There were no differences between cells treated with GNRs and irradiated with laser power of 1 W and 1.5 W and both were different from those treated with 2 W, this behavior can be explained considering that power of 2 W itself induce cellular death and along with the GNRs presents in the medium there is possibly a synergic effect that induce a higher decrease in cell viability.

4. Conclusions

Potential applications of polymeric material to construct functional devices are based on the capacity to tailor their chemical and physical properties. At this regard, we used three biocompatible and biodegradable polymers: thiolated chitosan (Chi-SH), alginate (Alg) and polyvinyl alcohol (PVA) to overcoat the surface of gold nanorods (GNR), following a two sequential steps coating process. First, Chi-SH was used to overcoat the surface of GNR and stabilized it, removing the CTAB from its surface. The Chi-SH layer deposited onto the GNR surface allows to obtain a non-cytotoxic GNR system potentially useful for medical purposes as photothermal agent. The adsorption of Chi-SH onto the surface of GNRs resulted in a versatile nanosystem with available reactive chemical functional groups (—NH and —OH) bound to the chitosan backbone that allow tune the physicochemical properties of the Chi-SH-GNR surface. Nevertheless, the application of Chi-SH-GNR in medical field is limited by the pKa (pH = 6.3) of chitosan that drives the

protonation-deprotonation of amine groups. Thus, at physiological pH amine groups are deprotonated, changing the surface charge of Chi-SH-GNR from +34 mV near to zero which resulted in the aggregation of Chi-SH-GNRs. To provide stability at the physiological pH, the surface of Chi-SH-GNRs was overcoated with alginate or PVA, changing the surface charge from positive to highly negative (Alg-Chi-SH-GNR) or slightly negative (PVA-Chi-SH-GNR), respectively. In accord to cellular assays both Alg-Chi-SH-GNR and PVA-Chi-SH-GNR did not affect significantly the cellular viability, in contrast to the high cytotoxic effect observed for CTAB-GNR. In order to have knowledge about their potential as photothermal agents, the photothermal conversion efficacy (η) of these GNR systems was evaluated. Interestingly, the η values determined for Chi-SH-GNR, Alg-Chi-SH-GNR and PVA-Chi-SH-GNR are at around 50% and similar to the η value for CTAB-GNR obtained in the present and previous reports. In addition, the cell viability was greatly affected when cell cultures, in presence of polymeric coated GNRs, were irradiated with CW laser (808 nm), as result of the photothermal heating around GNRs. Based on the present results, polymeric GNR systems have a potential use in biomedical areas because of their chemical, physical and photothermic properties. Specifically, we considered that Alg-Chi-SH-GNR and PVA-Chi-SH-GNR to be the most adequate nanosystem for biomedical purposes, since they present high stability in PBS buffer and cell media culture.

4.1. Outlooks

In addition to photothermal properties of Chi-SH-GNR, Alg-Chi-SH-GNR and PVA-Chi-SH-GNR fabricated in the present research work, currently we are focused in the bioactive modulation of these polymer coated systems by the addition of a chemotherapeutic agent, such as cis-platinum. Additionally, we are attempting modify the surface of Chi-SH-, Alg-Chi-SH- and PVA-Chi-SH-GNR by the covalent attachment of specific molecular targeting (PEPTIDES) in order to improve the adhesion and the internalization to specific cellular line. Finally, in vitro and, possibly, in vivo tests will be developed to prove their potential therapeutic properties.

Acknowledgment

We would like to thank the CONACYT (México) No. 236185 and CONACYT/CONICYT (México) No. 204393, CONICYT/CONACYT (Chile) No. 130048 and FONDECYT (Chile) No. 3140489 for their financial support. Mario Almada thanks CONACyT for the Ph. D. scholarship.

Appendix A. Supplementary data

Supplementary data to this article can be found online at http://dx.doi.org/10.1016/j.msec.2017.03.218.

References

[1] G.V. Hartland, Optical studies of dynamics in noble metal nanostructures, Chem. Rev. 111 (2011) 3858–3887, http://dx.doi.org/10.1021/cr1002547.
[2] X. Huang, M.A. El-Sayed, Plasmonic photo-thermal therapy (PPTT), Alex. J. Med. 47 (2011) 1–9, http://dx.doi.org/10.1016/j.ajme.2011.01.001.
[3] D. Jaque, L. Martínez Maestro, B. del Rosal, P. Haro-Gonzalez, A. Benayas, J.L. Plaza, E. Martín Rodríguez, J. García Solé, Nanoparticles for photothermal therapies, Nano 6 (2014) 9494–9530, http://dx.doi.org/10.1039/c4nr00708e.
[4] F. Jabeen, M. Najam-ul-Haq, R. Javeed, C.W. Huck, G.K. Bonn, Au-nanomaterials as a superior choice for near-infrared photothermal therapy, Molecules 19 (2014) 20580–20593, http://dx.doi.org/10.3390/molecules191220580.
[5] S. Hwang, J. Nam, S. Jung, J. Song, H. Doh, S. Kim, Gold nanoparticle-mediated photothermal therapy: current status and future perspective, Nanomedicine (London) 9 (2014) 2003–2022, http://dx.doi.org/10.2217/nnm.14.147.
[6] G. Von Maltzahn, J. Park, A. Agrawal, N.K. Bandaru, K. Sarit, M.J. Sailor, S.N. Bhatia, Computationally guided photothermal tumor therapy using long-circulating gold nanorod antennas, Cancer Res. 69 (2009) 3892–3900, http://dx.doi.org/10.1158/0008-5472.CAN-08-4242.Computationally.
[7] X. Huang, S. Neretina, M.A. El-Sayed, Gold nanorods: from synthesis and properties to biological and biomedical applications, Adv. Mater. 21 (2009) 4880–4910, http://dx.doi.org/10.1002/adma.200802789.
[8] V.P. Pattani, J.W. Tunnell, Nanoparticle-mediated photothermal therapy: a comparative study of heating for different particle types, Lasers Surg. Med. 44 (2012) 675–684, http://dx.doi.org/10.1002/lsm.22072.
[9] Y. Hong, E. Lee, J. Choi, S.J. Oh, S. Haam, Y.M. Huh, D.S. Yoon, J.S. Suh, J. Yang, Gold nanorod-mediated photothermal modulation for localized ablation of cancer cells, J. Nanomater. 2012 (2012)http://dx.doi.org/10.1155/2012/825060.
[10] T.S. Hauck, A.A. Ghazani, W.C.W. Chan, Assessing the effect of surface chemistry on gold nanorod uptake, toxicity, and gene expression in mammalian cells, Small 4 (2008) 153–159, http://dx.doi.org/10.1002/smll.200700217.
[11] A.M. Alkilany, P.K. Nagaria, C.R. Hexel, T.J. Shaw, C.J. Murphy, M.D. Wyatt, Cellular uptake and cytotoxicity of gold nanorods: molecular origin of cytotoxicity and surface effects, Small 5 (2009) 701–708, http://dx.doi.org/10.1002/smll.200801546.
[12] C.M. Grabinski, N.M. Schaeublin, A. Wijaya, H. D'Couto, S.H. Baxamusa, K. Hamad-Schifferli, S.M. Hussain, Effect of gold nanorod surface chemistry on cellular response, ACS Nano 5 (2011) 2870–2879, http://dx.doi.org/10.1021/nn103476x.
[13] Y. Zhang, D. Xu, W. Li, J. Yu, Y. Chen, Effect of size, shape, and surface modification on cytotoxicity of gold nanoparticles to human HEp-2 and canine MDCK cells, J. Nanomater. 2012 (2012)http://dx.doi.org/10.1155/2012/375496.
[14] J. Wan, J.-H. Wang, T. Liu, Z. Xie, X.-F. Yu, W. Li, Surface chemistry but not aspect ratio mediates the biological toxicity of gold nanorods in vitro and in vivo, Sci. Rep. 5 (2015) 11398, http://dx.doi.org/10.1038/srep11398.
[15] T. Gong, D. Goh, M. Olivo, K.T. Yong, In vitro toxicity and bioimaging studies of gold nanorods formulations coated with biofunctional thiol-PEG molecules and pluronic block copolymers, Beilstein J. Nanotechnol. 5 (2014) 546–553, http://dx.doi.org/10.3762/bjnano.5.64.
[16] C. Gui, D.-X. Cui, Functionalized gold nanorods for tumor imaging and targeted therapy, Cancer Biol. Med. 9 (2012) 221–233, http://dx.doi.org/10.7497/j.issn.2095-3941.2012.04.002.
[17] Z. Zhang, J. Wang, C. Chen, Gold nanorods based platforms for light-mediated theranostics, Theranostics 3 (2013) 223–238, http://dx.doi.org/10.7150/thno.5409.
[18] T. Niidome, M. Yamagata, Y. Okamoto, Y. Akiyama, H. Takahashi, T. Kawano, Y. Katayama, Y. Niidome, PEG-modified gold nanorods with a stealth character for in vivo applications, J. Control. Release 114 (2006) 343–347, http://dx.doi.org/10.1016/j.jconrel.2006.06.017.
[19] C. Kinnear, H. Dietsch, M.J.D. Clift, C. Endes, B. Rothen-Rutishauser, A. Petri-Fink, Gold nanorods: controlling their surface chemistry and complete detoxification by a two-step place exchange, Angew. Chem. Int. Ed. 52 (2013) 1934–1938, http://dx.doi.org/10.1002/anie.201208568.
[20] Z. Zhang, M. Lin, Fast loading of PEG–SH on CTAB-protected gold nanorods, RSC Adv. 4 (2014) 17760–17767, http://dx.doi.org/10.1039/c3ra48061e.
[21] C. Kinnear, D. Burn, M.J.D. Clift, A.F.M. Kilbinger, B. Rothen-Rutishauser, A. Petri-Fink, Polyvinyl alcohol as a biocompatible alternative for the passivation of gold nanorods, Angew. Chem. Int. Ed. 53 (2014) 12613–12617, http://dx.doi.org/10.1002/anie.201404100.
[22] D. Pissuwan, T. Niidome, Polyelectrolyte-coated gold nanorods and their biomedical applications, Nano 7 (2015) 59–65, http://dx.doi.org/10.1039/c4nr04350b.
[23] C.H. Wang, C.W. Chang, C.A. Peng, Gold nanorod stabilized by thiolated chitosan as photothermal absorber for cancer cell treatment, J. Nanopart. Res. 13 (2011) 2749–2758, http://dx.doi.org/10.1007/s11051-010-0162-5.
[24] S. Charan, K. Sanjiv, N. Singh, F.C. Chien, Y.F. Chen, N.N. Nergui, S.H. Huang, C.W. Kuo, T.C. Lee, P. Chen, Development of chitosan oligosaccharide-modified gold nanorods for in vivo targeted delivery and noninvasive imaging by NIR irradiation, Bioconjug. Chem. 23 (2012) 2173–2182, http://dx.doi.org/10.1021/bc3001276.
[25] Z. Yang, T. Liu, Y. Xie, Z. Sun, H. Liu, J. Lin, C. Liu, Z.W. Mao, S. Nie, Chitosan layered gold nanorods as synergistic therapeutics for photothermal ablation and gene silencing in triple-negative breast cancer, Acta Biomater. 25 (2015) 194–204, http://dx.doi.org/10.1016/j.actbio.2015.07.026.
[26] K.Y. Lee, D.J. Mooney, Alginate: properties and biomedical applications, Prog. Polym. Sci. 37 (2012) 106–126, http://dx.doi.org/10.1016/j.progpolymsci.2011.06.003.
[27] M.K. Pati, D. Dash, M.K. Pati, Chitosan: a versatile biopolymer for various medical applications, Int. J. Sci. Eng. Res. 4 (2013) 1–16.
[28] A. Nasti, N.M. Zaki, P. De Leonardis, S. Ungphaiboon, P. Sansongsak, M.G. Rimoli, N. Tirelli, Chitosan/TPP and chitosan/TPP-hyaluronic acid nanoparticles: systematic optimisation of the preparative process and preliminary biological evaluation, Pharm. Res. 26 (2009) 1918–1930, http://dx.doi.org/10.1007/s11095-009-9908-0.
[29] W. Fan, W. Yan, Z. Xu, H. Ni, Erythrocytes load of low molecular weight chitosan nanoparticles as a potential vascular drug delivery system, Colloids Surf. B: Biointerfaces 95 (2012) 258–265, http://dx.doi.org/10.1016/j.colsurfb.2012.03.006.
[30] Y. Huang, Y. Cai, Y. Lapitsky, Factors affecting the stability of chitosan/tripolyphosphate micro- and nanogels: resolving the opposing findings, J. Mater. Chem. B 3 (2015) 5957–5970, http://dx.doi.org/10.1039/C5TB00431D.
[31] J. Zhu, K.-T. Yong, I. Roy, R. Hu, H. Ding, L. Zhao, M.T. Swihart, G.S. He, Y. Cui, P.N. Prasad, Additive controlled synthesis of gold nanorods (GNRs) for two-photon luminescence imaging of cancer cells, Nanotechnology 21 (2010) 285106, http://dx.doi.org/10.1088/0957-4484/21/28/285106.
[32] M. Almada, E.D. Ruiz, J. Ibarra-Hurtado, N. Hassan, M.J. Kogan, R.D. Cadena-Nava, M.A. Valdés, J. Juárez, Growth kinetics of gold nanorods synthesized by a seed-mediated method under pH acidic conditions, J. Nanosci. Nanotechnol. 16 (2016) 7707–7714, http://dx.doi.org/10.1166/jnn.2016.12438.
[33] X. Zhu, M. Su, S. Tang, L. Wang, X. Liang, F. Meng, Y. Hong, Z. Xu, Synthesis of thiolated chitosan and preparation nanoparticles with sodium alginate for ocular drug delivery, Mol. Vis. 18 (2012) 1973–1982.

[34] D.K. Roper, W. Ahn, M. Hoepfner, Microscale heat transfer transduced by surface plasmon resonant gold nanoparticles, J. Phys. Chem. C 111 (2007) 3636–3641, http://dx.doi.org/10.1021/jp064341w.
[35] K.S. Lee, M.A. El-Sayed, Dependence of the enhanced optical scattering efficiency relative to that of absorption for gold metal nanorods on aspect ratio, size, end-cap shape, and medium refractive index, J. Phys. Chem. B 109 (2005) 20331–20338, http://dx.doi.org/10.1021/jp054385p.
[36] A. Brioude, X.C. Jiang, M.P. Pileni, Optical properties of gold nanorods: DDA simulations supported by experiments, J. Phys. Chem. B 109 (2005) 13138–13142, http://dx.doi.org/10.1021/jp0507288.
[37] P.K. Jain, K.S. Lee, I.H. El-Sayed, M.A. El-Sayed, Calculated absorption and scattering properties of gold nanoparticles of different size, shape, and composition: applications in biological imaging and biomedicine, J. Phys. Chem. B 110 (2006) 7238–7248, http://dx.doi.org/10.1021/jp057170o.
[38] R.D. Near, S.C. Hayden, R.E. Hunter, D. Thackston, M.A. El-Sayed, Rapid and efficient prediction of optical extinction coefficients for gold nanospheres and gold nanorods, J. Phys. Chem. C 117 (2013) 23950–23955, http://dx.doi.org/10.1021/jp4082596.
[39] Z. Nie, D. Fava, E. Kumacheva, S. Zou, G.C. Walker, M. Rubinstein, Self-assembly of metal-polymer analogues of amphiphilic triblock copolymers, Nat. Mater. 6 (2007) 609–614, http://dx.doi.org/10.1038/nmat1954.
[40] M. Sethi, G. Joung, M.R. Knecht, Linear assembly of Au nanorods using biomimetic ligands, Langmuir 25 (2009) 1572–1581, http://dx.doi.org/10.1021/la802845b.
[41] L. Wang, Y. Zhu, L. Xu, W. Chen, H. Kuang, L. Liu, A. Agarwal, C. Xu, N.A. Kotov, Side-by-side and end-to-end gold nanorod assemblies for environmental toxin sensing, Angew. Chem. Int. Ed. 49 (2010) 5472–5475, http://dx.doi.org/10.1002/anie.200907357.
[42] A. Lee, A. Ahmed, D.P. Santos, N. Coombs, J. Il Park, R. Gordon, A.G. Brolo, E. Kumacheva, Side-by-side Assembly of Gold Nanorods Reduces Ensemble-Averaged SERS Intensity, Scanning, 2012.
[43] C. Adura, S. Guerrero, E. Salas, L. Medel, A. Riveros, J. Mena, J. Arbiol, F. Albericio, E. Giralt, M.J. Kogan, Stable conjugates of peptides with gold nanorods for biomedical applications with reduced effects on cell viability, ACS Appl. Mater. Interfaces 5 (2013) 4076–4085.
[44] D.I. Gittins, F. Caruso, Tailoring the polyelectrolyte coating of metal nanoparticles, J. Phys. Chem. B 105 (2001) 6846–6852, http://dx.doi.org/10.1021/jp0111665.
[45] Luis L.-M., V. Salgueiriño-Maceira, F. Caruso, Coated colloids with tailored optical properties, J. Phys. Chem. B 107 (2003) 10990–10994, http://dx.doi.org/10.1021/jp034302.
[46] K.S. Mayya, B. Schoeler, F. Caruso, Preparation and organization of nanoscale polyelectrolyte-coated gold nanoparticles, Adv. Funct. Mater. 13 (2003) 183–188, http://dx.doi.org/10.1002/adfm.200390028.
[47] A. Gole, C.J. Murphy, Polyelectrolyte-coated gold nanorods: synthesis, characterization and immobilization, Chem. Mater. 17 (2005) 1325–1330, http://dx.doi.org/10.1021/cm048297d.
[48] B.-S. Choi, M. Iqbal, T. Lee, Y.H. Kim, G. Tae, Removal of cetyltrimethylammonium bromide to enhance the biocompatibility of Au nanorods synthesized by a modified seed mediated growth process, J. Nanosci. Nanotechnol. 8 (2008) 4670–4674, http://dx.doi.org/10.1166/jnn.2008.IC18.
[49] A. Shokuhfar, S.S.S. Afghahi, The heating effect of iron-cobalt magnetic nanofluids in an alternating magnetic field: application in magnetic hyperthermia treatment, Nanoscale Res. Lett. 8 (2013) 1–25, http://dx.doi.org/10.1186/1556-276X-8-540.
[50] L. Jin, R. Bai, Mechanisms of lead adsorption on chitosan/PVA hydrogel beads, Langmuir 18 (2002) 9765–9770, http://dx.doi.org/10.1021/la025917l.
[51] M. Almada, M.G. Burboa, E. Robles, L.E. Gutiérrez, M.A. Valdés, J. Juárez, Interaction and cytotoxic effects of hydrophobized chitosan nanoparticles on MDA-MB-231, HeLa and Arpe-19 cell lines, Curr. Top. Med. Chem. 14 (2014) 692–701, http://dx.doi.org/10.2174/1568026614666140118214802.
[52] C. Le Tien, M. Lacroix, P. Ispas-Szabo, M.A. Mateescu, N-acylated chitosan: hydrophobic matrices for controlled drug release, J. Control. Release 93 (2003) 1–13, http://dx.doi.org/10.1016/S0168-3659(03)00327-4.
[53] H.S. Mansur, C.M. Sadahira, A.N. Souza, A.A.P. Mansur, FTIR spectroscopy characterization of poly (vinyl alcohol) hydrogel with different hydrolysis degree and chemically crosslinked with glutaraldehyde, Mater. Sci. Eng. C 28 (2008) 539–548, http://dx.doi.org/10.1016/j.msec.2007.10.088.
[54] G. Lawrie, I. Keen, B. Drew, A. Chandler-Temple, L. Rintoul, P. Fredericks, L. Grøndahl, Interactions between alginate and chitosan biopolymers characterized using FTIR and XPS, Biomacromolecules 8 (2007) 2533–2541, http://dx.doi.org/10.1021/bm070014y.
[55] K. Draget, O. Smidsrød, G. Skjåk-Bræk, Alginates From Algae, Pollysaccharides Plyamides Food Ind. Prop. Prod. Patents, 2005 1–30, http://dx.doi.org/10.1002/3527600035.bpol6008.
[56] T. Harnsilawat, R. Pongsawatmanit, D.J. McClements, Characterization of beta-lactoglobulin-sodium alginate interactions in aqueous solutions: a calorimetry, light scattering, electrophoretic mobility and solubility study, Food Hydrocoll. 20 (2006) 577–585, http://dx.doi.org/10.1016/j.foodhyd.2005.05.005.
[57] H. Chen, L. Shao, T. Ming, Z. Sun, C. Zhao, B. Yang, J. Wang, Understanding the photothermal conversion efficiency of gold nanocrystals, Small 6 (2010) 2272–2280, http://dx.doi.org/10.1002/smll.201001109.
[58] K. Jiang, D.A. Smith, A. Pinchuk, Size-dependent photothermal conversion efficiencies of plasmonically heated gold nanoparticles, J. Phys. Chem. C 117 (2013) 27073–27080, http://dx.doi.org/10.1021/jp409067h.
[59] M.A. Mackey, M.R.K. Ali, L.A. Austin, R.D. Near, M.A. El-sayed, The most effective gold nanorod size for plasmonic photothermal therapy: theory and in vitro experiments the most effective gold nanorod size for plasmonic photothermal therapy: theory and in vitro experiments, J. Phys. Chem. B 118 (2014) 1319–1326, http://dx.doi.org/10.1021/jp409298f.
[60] J.R. Cole, N.A. Mirin, M.W. Knight, G.P. Goodrich, N.J. Halas, Photothermal efficiencies of nanoshells and nanorods for clinical therapeutic applications, J. Phys. Chem. C 113 (2009) 12090–12094, http://dx.doi.org/10.1021/jp9003592.
[61] D. Pissuwan, S. Valenzuela, M.B. Cortie, Prospects for gold nanorod particles in diagnostic and therapeutic applications, Biotechnol. Genet. Eng. Rev. 25 (2008) 93–112, http://dx.doi.org/10.5661/bger-25-93.
[62] M. George, T.E. Abraham, Polyionic hydrocolloids for the intestinal delivery of protein drugs: alginate and chitosan - a review, J. Control. Release 114 (2006) 1–14, http://dx.doi.org/10.1016/j.jconrel.2006.04.017.
[63] A. Rafiee, M.H. Alimohammadian, T. Gazori, F. Riazi-rad, S.M.R. Fatemi, A. Parizadeh, I. Haririan, M. Havaskary, Comparison of chitosan, alginate and chitosan/alginate nanoparticles with respect to their size, stability, toxicity and transfection, Asian Pac. J. Trop. Dis. 4 (2014) 372–377, http://dx.doi.org/10.1016/S2222-1808(14)60590-9.
[64] M.I. Baker, S.P. Walsh, Z. Schwartz, B.D. Boyan, A review of polyvinyl alcohol and its uses in cartilage and orthopedic applications, J. Biomed. Mater. Res. B Appl. Biomater. 100 (B) (2012) 1451–1457, http://dx.doi.org/10.1002/jbm.b.32694.